



GEOGRID REINFORCEMENT IN FLEXIBLE PAVED ROADS

Ahmed, Mai^{1,2}, Abdelhamid, Mennatallah¹, Hussain, Sarah¹, Khedr, Safwan¹, Breakah, Tamer¹, Saudy, Maram¹, Elkadi, Omar¹, Abou-Zeid, Mohamed¹

¹ The Department of Construction Engineering, The American University In Cairo, Egypt

²Mai_ibrahim@aucegypt.edu

Abstract: The scope of this study is to explore and evaluate the effect of reinforcing the interface between the base and asphalt concrete layers in a flexible pavement section with bi-axial geogrids; using both large scale experimental tests and numerical modeling using three-dimensional nonlinear finite elements analysis. A laboratory characterization for each layer of the pavement section according to a laboratory programs that included soil classification, plate loading test, determination of asphalt concrete dynamic modulus for and CBR ratio for different elements in pavement section. A laboratory model of the pavement with and without the geogrid reinforcement, located at the top of the base layer was constructed. A dynamic loading scheme was applied on the experimental pavement model. Concurrently, a numerical model was developed to simulate the effect of such type of reinforcement on the pavement section in terms of the road's performance enhancement and reduction in rutting. The numerical model was proved to verify simulation of the pavement experimental model when comparing the overall trend of stress distribution throughout the pavement structure.

1 INTRODUCTION

Geogrids are one type of geosynthetic reinforcement systems. They are made of polymers that are connected in parallel sets of tensile ribs with openings in between them (Abu-Farsakh, 2016). According to literature, geogrids can effectively decrease rutting in the asphalt concrete layer in flexible pavement (Gu, 2016). This may be attributed to the mechanism of the geogrids interaction with the pavement layers (Moghaddas-Nejad, 1996). When the asphalt concrete layer is compacted over geogrids, the aggregate particles penetrate through the openings of the grid resulting in the creation of a strong interlock and therefore the lateral movements of the unbound base material or mix particles are reduced drastically. This interlock acts as a resistor for rutting development such that stresses are transferred by tensile forces and thus the performance of the road is enhanced (Abu-Farsakh, 2011).

Geogrid reinforcement is utilized as a part of flexible paved roadways in two noteworthy application zones: base reinforcement and subgrade stabilization Limited research has been conducted on base reinforcement applications, so the scope of this research was to explore and test the effect of reinforcing the interface between the base and the asphalt concrete layers in a flexible pavement section using bi-axial geogrids.

The methodology of this research was divided into two phases; experimental work and numerical modeling. The experimental work consisted of lab characterization of the different materials used in the different layers of flexible pavement; namely, untreated base, subgrade soil, geogrid and asphalt concrete. A full scale pavement laboratory model was subjected to dynamic loading, simulating traffic

loads on a road. The pavement section structure was decided through proper conventional design analysis. Iterations and trials on the finite element modeling software “MIDAS” were used in order to simulate the effect of geogrids on the paved road section using a 3D model and verified by the full scale dynamic testing.

2 EXPERIMENTAL PROGRAM

2.1 Lab Materials Characterization

Different tests were conducted on the various layers of the pavement section in order to measure and determine the parameters to be used to characterize the layers as input to the numerical model. The results are shown in Table 1. Properties that were not tested were reasonably assumed based on previous experiences as well as from the literature.

Table 1: Small Scale Tests

Layer	Test Name	ASTM
Subgrade	Gradation	C136/C136M - 14
	Water Content	D2216-98
	Compaction	D698-12e2
	CBR	D1883-16
	Specific Gravity	D854-14
	Direct Shear	D3080
Base	Gradation	C136/C136M - 14
	Water Content	D2216-10
	Modified Proctor Compaction	D1557-12
	CBR	D1883-16
	Specific Gravity	C127-15
Asphalt Concrete	Flow and Stability	D6927-15
	Extraction	D2172/D2172M-17
	Theoretical Maximum Specific Gravity (G_{mm})	D2041/D2041M-11
	Dynamic Modulus (E^*)	D3497
	Tensile Strength	D6637
Geogrids (Tenax LBO 330)		

2.1.1 Materials Properties

Soil, base material and asphalt mix constituents were obtained from a construction site. Tables 2 to 4 shows the measured characteristics of the materials used as subgrade, base and asphalt concrete for the tested model pavement section.

Table 2: Subgrade Layer Properties

Property	Result
Specific Gravity	2.70
Optimum Water Content (%)	7.6
$\gamma_{dry, max}$ (kN/m^3)	17.76
CBR (%)	26
Modulus of Elasticity (E), (MPa)	15.8
Cohesion (C)	0
Angle of Internal Friction (ϕ°)	30
Unit Weight in Full Scale Exp Model, (kN/m^3)	18
Poisson's Ratio (ν) (assumed)	0.3

Table 3: Base Layer Properties

Property	Result
AASHTO Classification	A
Specific Gravity	2.56
CBR (%)	142.7
Modulus of Elasticity (E) (MPa)	22
Angle of Internal Friction (ϕ°)	40
Unit Weight in Full Scale Exp Model, (kN/m ³)	20
Poisson's Ratio (ν) (assumed)	0.35

Table 4: Asphalt Concrete Layer Properties

Property	Result
Flow (2.5mm)	10.8
Stability (kN)	1.8
Optimum Asphalt Content (%)	5.66
Maximum Specific Gravity G_{mb}	2.1
Theoretical Maximum Specific Gravity (G_{mm})	2.41
Air Voids (Core Sample) (%)	13.7
Dynamic Modulus (E^*) (MPa)	161.5
Unit Weight in Full Scale Exp Model, (kN/m ³)	22
Poisson's Ratio (ν) (assumed)	0.45

Table 5: Geogrids Layer Properties

Property	Result
Tensile Strength (kN/m)	40.9
Modulus of Elasticity (MPa)	161.5
Unit Weight (kN/m ³)	1
Poisson's Ratio (ν) (assumed)	0.15

2.2 Full Scale Test

2.2.1 Test Design

Two full-scale pavement structures were tested; a control section and a geogrid reinforced section. The geogrids were placed in between the asphalt concrete layer and the base layer. The lab model had dimensions of 2x2x1 meters. The model boundaries did not significantly interfere with the pavement stress distribution as checked by the numerical model (MIDAS). The layers' thicknesses were selected in accordance to the Egyptian code of design, which suggested typical section with 10 cm of asphalt concrete and 25 cm of untreated base. This left subgrade soil layer of 65 cm in the lab model.

To achieve the desired degree of compaction, the weights according to maximum unit weight were prepared and compacted till pre-marked depth. Compaction was done using a plate compactor. The subgrade layer was divided and compacted on 3 layers: 0.25, 0.25, and 0.15 m. The degree of compaction for the subgrade using sand cone test was 102%. The base layer was divided and compacted on 2 layers, 12.5 cm each. The degree of compaction for the base layer was 100.23%. Asphalt concrete layer was placed and compacted on 2 layers, 5 cm thick each.

2.2.2 Test Setup

As shown in figure 1, the test setup comprises an actuator, external LVDTs, a loading plate, a data logger, and the full-scale tank.



a. Actuator and LVDT



b. Complete Test Setup

Figure 1: Full Scale Test Setup

2.2.3 Dynamic Load Pattern

The load pattern chosen is shown in Figure 2. This loading simulated the load of vehicles at intersections, toll stations and slow speed roads. It was selected because rutting increases at these locations of the roads and the asphalt concrete becomes more vulnerable to the applied loads of the trucks than in the locations of higher speeds. Each loading cycle lasted for one second in which:

- 0.2 second of constant load of 0.5 ton
- 0.3 second of loading from 0.5 ton to 10 tons
- 0.3 second of unloading from 10 tons to 0.5 ton
- 0.2 second of constant load of 0.5 ton

The minimum load which is the 0.5 ton was used instead of zero load to avoid the impact due to load application.

The load pattern was assigned through the control system of the actuator. Five thousand loading cycles were applied and stopped for the hydraulic pump to cool down and then the next 5000 cycles were applied and so on.

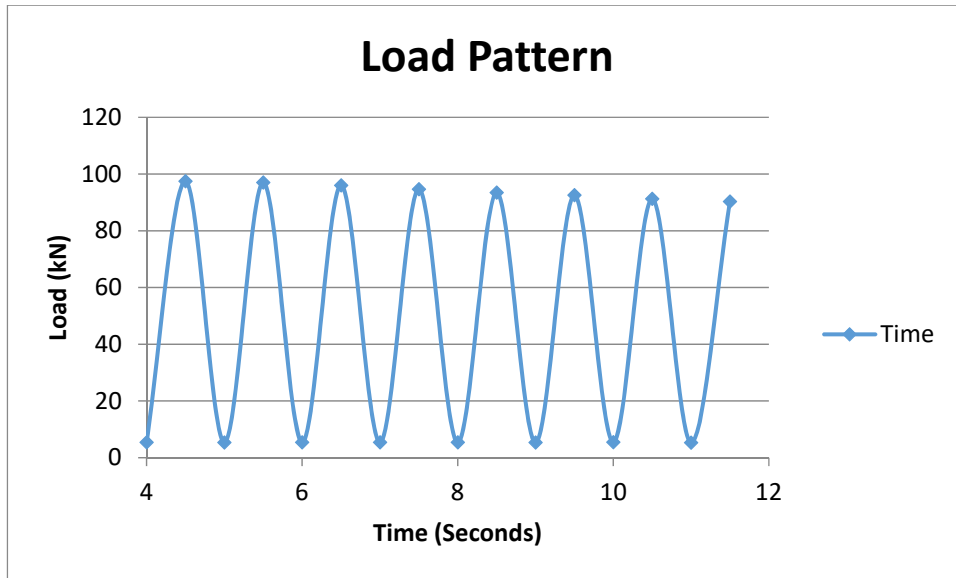


Figure 2: Load Pattern

2.2.4 Number Of Cycles

The applied maximum load of 10 tons (98 kN) was converted to ESALs using the ESAL equivalency table presented in the Egyptian Code of Design and AASHTO 1995. The total load on an axle was 200kN and thus each loading cycle was equivalent to 39 ESALs. The test was continued up to 30,000 cycle, which means that the maximum ESALs applied throughout the test was 1,170,000 for each of the test setups.

2.2.5 Tire Contact Area

According to previous research, a loading area size of 0.31 x 0.20 m was used to simulate the loading imprint.

2.2.6 Pressure Gauges Setup

To observe and study the stresses distribution in the different layers of the road, ten pressure gauges were placed inside the full scale model. The pressure gauges were placed at different positions as shown in Figure 3. The pressure gauges were labelled from P1 to P10. The distribution is clarified in the figure (P1 and P8 were placed laterally in order to measure vertical pressures).

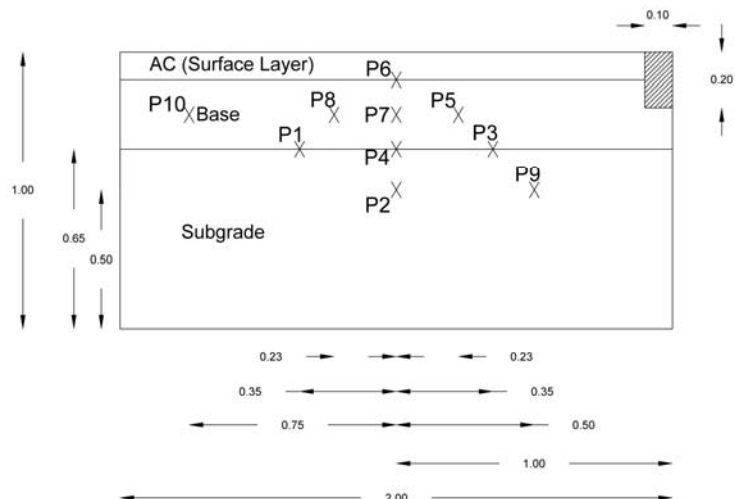


Figure 3: Pressure Gauges Locations (Elevation)

2.2.7 Full Scale Model Testing Results

The rutting results were acquired from mounted LVDT's. The readings were taken each 50 milliseconds, and the readings included time and load, which was measured by a load cell and deformation. The residual deformation for each 5000 cycles was subtracted from the values obtained for the next 5000 cycles to get the plastic deformation caused by the load. This modification was made to the 30,000 cycles to be able to get the plastic deformation at each load throughout the 30,000 cycles.

The modified deformation versus cycle curve is shown in Figure 4.

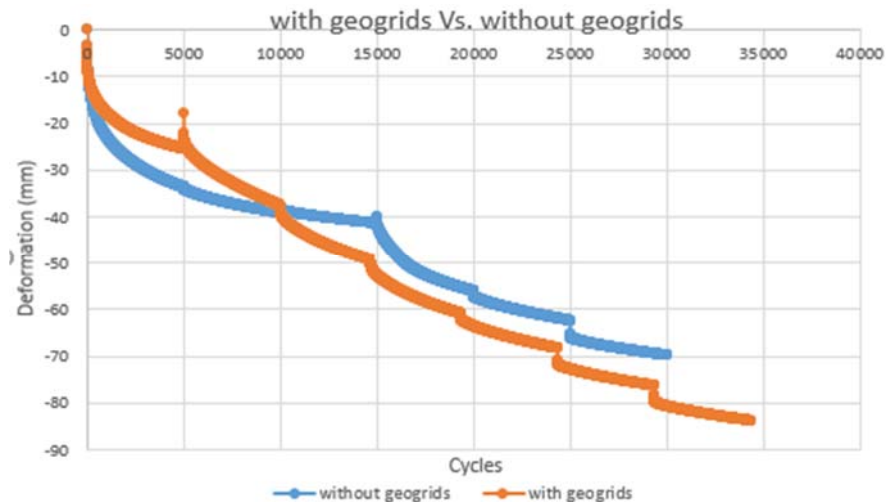


Figure 4: Modified Deformation versus Cycles Graph

When comparing the results of the two models, it was observed that the sample with geogrids had less deformation until cycle number 10,000. The area before the cycle 10,000 is the area that should be analyzed because the rutting appeared in the sample without geogrids in the cycle 1000, which is equivalent to 39,000 ESALs.

By visual inspection to the model without geogrids, after the asphalt layer was removed, an apparent deformation in the base layer was found. This can be explained that the stresses were carried by the base layer rather than the asphalt layer, which led to lower deformation as after the cycle number 10,000, and this shows the stresses dissipation through the asphalt concrete layer.

For the sample with geogrids, the asphalt layer and the geogrids carried all the stresses, which was proved when the asphalt layer was removed and no deformation in the base layer was found.

In the sample without geogrids, after 1000 cycles, the rutting had already appeared which means that the asphalt already reached failure condition. While in the sample with geogrids, the rutting started to appear in the asphalt layer after nearly 3000 cycles, which is equivalent to 117,000 ESALs. This means that geogrids tripled the lifetime of the asphalt.

The deformation of the LVDT was used to plot the deformation against time for loading cycles to show the resilient deformation that happened within the cycle as the load was added and then removed and the residual deformation that is accumulated through the loading cycles as shown in Figure 5.

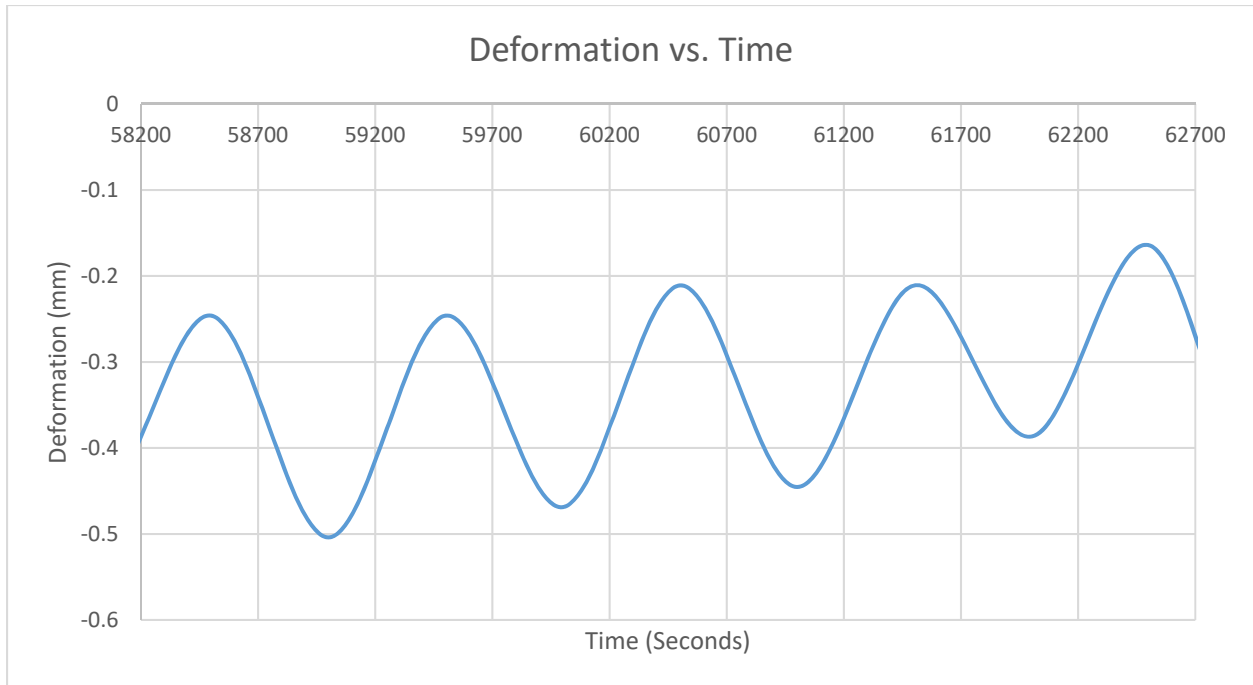


Figure 5: Deformation versus Time Graph

2.2.8 Rutting

The total rutting deformation for the control section was 7.3cm and for the reinforced section was 5.2cm. The shape of the models after the end of the test is shown in Figure 6.



a) Without Geogrids



b) With Geogrids

Figure 6: Rutting Appearance

3 NUMERICAL MODELING

3.1 Preliminary Model

A preliminary model with assumed material properties was firstly developed to decide on the boundary conditions of the tank that were needed to be fabricated for the full-scale test.

A table for the constitutive models used and the mesh sizes used for the model is as follows:

Table 6: Constitution Models and Mesh Sizes Table

Layer	Mesh Size (m)	Constitutive Model
Subgrade	0.2	Mohr-Coulomb
Base	0.15	Mohr-Coulomb
Asphalt Concrete	0.12	Elastic

Several iterations were done to reach the model dimensions. The selected dimensions were 2 x 2 x 1 m, results showed that the boundary conditions did not significantly affect the stresses. It also showed that the deformation is negligible at the sides of the tank, which means the 2 x 2 m dimension of the tank is sufficient and that the deformation is not affected by the height of the tank, which is 1 meter high. The vertical deformation of the cross section as calculated in the numerical model is shown in Figure 7.

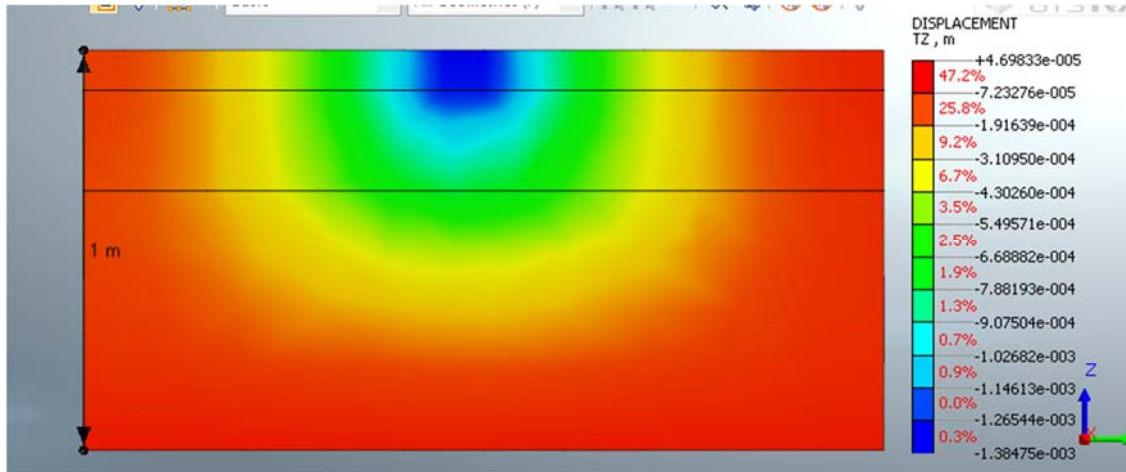


Figure 7: Cross-section for the vertical deformation

3.2 Final Model

After the full-scale test, another two models were developed for both the lab model with geogrids and the sample without geogrids. The model was based on an equivalent static load analysis, where the dynamic modulus of the asphalt was used.

3.2.1 Without Geogrids

The results showed that the stresses are highest at the center of loading and decreases towards the sides, thus; the deformation is maximum at the center and decreases towards the sides. The model also showed the points where plastic points had occurred which means that there is plastic deformation at these points and they will not return back to their positions. The results of the model are shown in Figure 8.

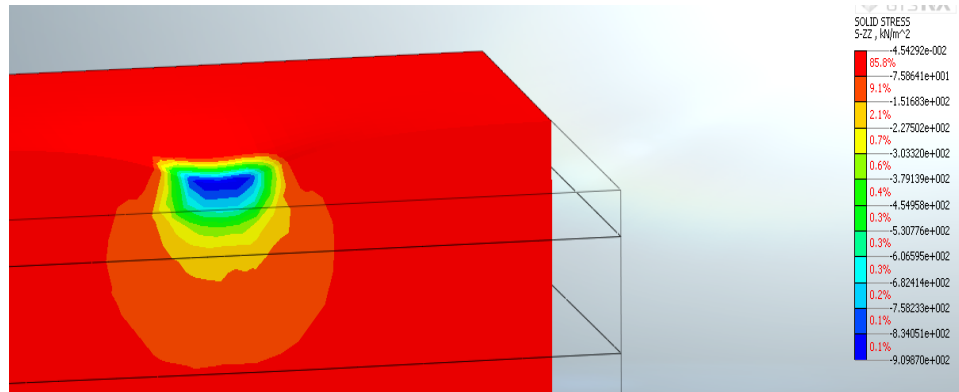


Figure 8: Cross-section for the vertical stresses

3.2.2 With Geogrids

The model with geogrids showed a better stress distribution than that of the sample with no geogrids as the geogrids helped in distribution of forces through tensioning the geogrids which also caused interlocking of particles in the asphalt layer, thus, resulting in a better distribution of stresses in the base layer. The results of the model are shown in Figure 9.

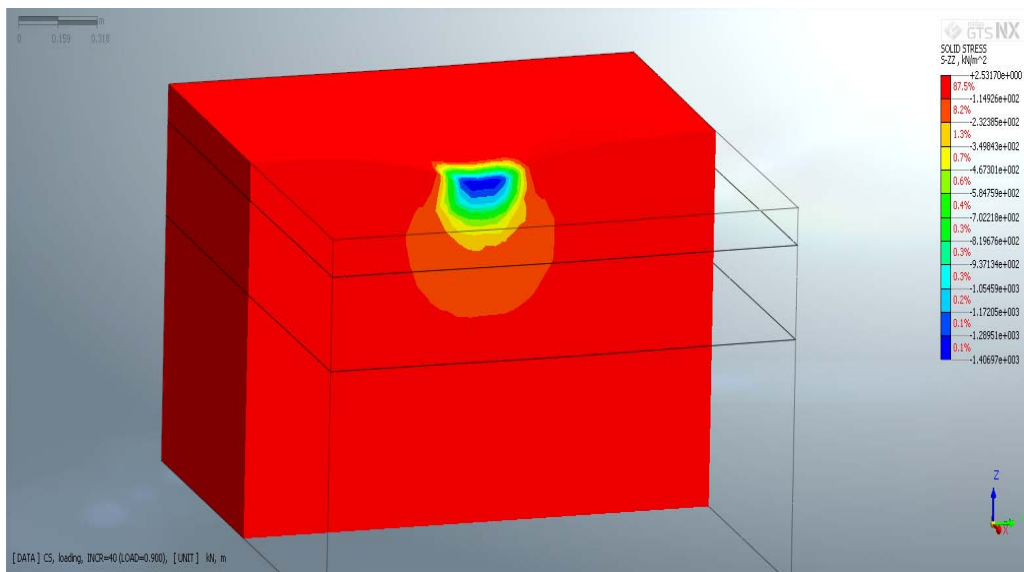


Figure 9: Cross-section for the Vertical Stresses

The model with geogrids also illustrated the tension that occurred in the geogrids layer and how the forces are distributed in the xx direction. The tension in the geogrids caused an interlocking of particles of the asphalt that lead to better distribution of stresses.

4 ANALYSIS OF RESULTS

The interpretation of the full-scale test results and visual inspection showed occurrence of residual deformation in the base layer with the absence of geogrids. Adding geogrids decreased this phenomenon and consequently reduced pavement rutting significantly (almost 30% less). The experimental model was modeled afterwards on MIDAS Software with and without geogrids. The model without geogrids showed a numerical failure at 60% of the load, which means that the model failed to find convergence due to instability; thus, the asphalt failed. However, the numerical failure in

the model with geogrids was at 90% of the load. The numerical failure difference indicates that the geogrids caused 30% enhancement in terms of the pavement load carrying capacity.

A better distribution of stresses in the model with geogrids was observed, since the geogrids led to the interlock of particles of the asphalt. The results of the model could not be numerically compared to that of the full-scale test because the numerical model was based on an equivalent static load analysis and the full-scale test was done based on dynamic loading. However, the overall trend of stress distribution was the same in both the full-scale test and the model.

5 CONCLUSION

From the results and analysis stated above, it was concluded that the geogrids had a major effect on the stresses distribution inside the section of the road tested, as the stresses did not cause a deformation in the base layer in the case of presence of the geogrids. Additionally, from the full-scale test it was concluded that the presence of geogrids increases the lifetime of the asphalt concrete by nearly three times.

6 RECOMMENDATIONS

For further research, it is recommended to:

1. Evaluate the Fatigue Cracking caused by the cyclic loading
2. Try using Geogrids in different positions, which may enhance the results of the stresses
3. Test the dynamic modulus at different temperatures instead of testing it at the only one temperature, to account for the change in the properties of the asphalt concrete due to climate changes
4. Test the exact shear properties of the Subgrade and Base layer rather than using reasonable assumptions
5. Modeling the full-scale test using dynamic loading instead of equivalent static loading on MIDAS

References

- Abu-Farsakh, Murad, Shadi Hanandeh, Louay Mohammad, and Qiming Chen. "Performance of geosynthetic reinforced/stabilized paved roads built over soft soil under cyclic plate loads." *Geotextiles and Geomembranes* 44, no. 6 (2016): 845-53. doi:10.1016/j.geotexmem.2016.06.009.
- Abu-Farsakh, Murad Y., and Qiming Chen. "Evaluation of geogrid base reinforcement in flexible pavement using cyclic plate load testing." *International Journal of Pavement Engineering* 12, no. 3 (2011): 275-88. doi:10.1080/10298436.2010.549565.
- American Association of State Highway and Transportation Officials. 1995. AASHTO provisional standards. Washington, D.C.: American Association of State Highway and Transportation Officials.
- Breakah, Tamer M., and R. Christopher Williams. "Stochastic finite element analysis of moisture damage in hot mix asphalt." *Materials and Structures* 48, no. 1-2 (2013): 93-106. doi:10.1617/s11527-013-0170-x.
- Gu, Fan, Xue Luo, Rong Luo, Robert L. Lytton, Elie Y. Hajj, and Raj V. Siddharthan. "Numerical modeling of geogrid-reinforced flexible pavement and corresponding validation using large-scale tank test." *Construction and Building Materials* 122 (2016): 214-30. doi:10.1016/j.conbuildmat.2016.06.081.
- Moghaddas-Nejad, Fereidoon, and John C. Small. "Closure to "Effect of Geogrid Reinforcement in Model Track Tests on Pavements" by Fereidoon Moghaddas-Nejad and John C. Small." *Journal of Transportation Engineering* 125, no. 3 (1999): 267. doi:10.1061/(asce)0733-947x(1999)125:3(267)